45. Nonlinear Optoelectronic Materials

In a nonlinear optical material, intense light alters the real and imaginary components of the refractive index. The nonlinear response of the real part of refractive index modifies the phase of propagating light, while the imaginary part describes the change in absorption. These illumination-dependent properties of nonlinear materials provide the basis for all-optical switching—the ability to manipulate optical signals without the need for optical–electronic–optical conversion.

In this chapter we review the physical processes underlying the illumination-dependent refractive index. We review the real and imaginary nonlinear response of representative groups of materials: crystalline semiconductors, organic materials, and nanostructures, and we examine the practical applicability of these groups of materials to all-optical optical switching. We identify the spectral regions which offer the most favorable nonlinear response as characterized using engineering figures of merit.

45.1 **Background** 1075
45.1.1 Signal Processing in Optical Networks 1075
45.1.2 Optical Signal Processing Using Nonlinear Optics 1076
45.1.3 The Approach Taken During this Survey of Nonlinear Optoelectronic Materials 1076
45.2 **Illumination-Dependent Refractive Index and Nonlinear Figures of Merit (FOM)** 1077
45.2.1 Ultrafast Response 1077
45.2.2 Ultrafast Nonlinear Material Figures of Merit 1078
45.2.3 Resonant Response 1079
45.2.4 Resonant Nonlinear Material Figures of Merit 1079
45.3 **Bulk and Multi-Quantum-Well (MQW) Inorganic Crystalline Semiconductors** 1080
45.3.1 Resonant Nonlinearities 1080
45.3.2 Nonresonant Nonlinearities in Inorganic Crystalline Semiconductors 1083
45.4 **Organic Materials** 1084
45.4.1 Resonant Nonlinear Response of Organic Materials 1085
45.4.2 Nonresonant Nonlinear Response of Organic Materials 1086
45.5 **Nanocrystals** 1087
45.6 **Other Nonlinear Materials** 1088
45.7 **Conclusions** 1089
References 1089

45.1 Background

Optical fiber provides a suitable medium in which it is possible to reach tremendous transmission rates over long distances [45.1]. The maximum information-carrying capacity has been estimated to be around 100 Tbps [45.2]. Very high data rates can be achieved using a combination of wavelength- and time-division multiplexing techniques (WDM and TDM). WDM involves sending many signals in parallel at closely spaced wavelengths along the same fiber, while TDM allows close spacing in time of bits in a single channel.

While there exist means to produce, transfer, and detect information at a very high bandwidth, there is a need for more agility in photonic networks.

The agility of present-day optical networks is limited by the electronic nature of a very important function: the processing of information-bearing signals. Signal processing is responsible for switching and routing traffic, establishing links, restoring broken links, and monitoring and managing the network.

45.1.1 Signal Processing in Optical Networks

At present, the important and functionally complex signal-processing operations of switching and routing are carried out electronically. Electronic signal processing imposes two significant limitations on the functionality of optical networks: cost and opacity. Signal switching and routing requires conversion of the optical information into electrical signals, processing in the electronic domain, and converting back to the optical domain before retransmission. Such an operation requires detection, retiming, reshaping, and regeneration at each switching and routing point. This necessitates complex and expensive electronic and electro-optical hardware at each routing and switching node. The use of electronic signal processing places strict requirements on the format of data streams transferred and processed, thus making the signal processing opaque. Repetition rates of optical signals, power levels, and packet lengths have to be standardized before they can be processed electronically.

The ability to perform signal processing operations entirely within the optical domain would eliminate the requirement for optical–electrical–optical conversions, while providing agility and speed inherent to optical elements. Optical signal processing, in contrast with electronics, may provide ultrafast sub-picosecond switching times [45.3].

45.1.2 Optical Signal Processing Using Nonlinear Optics

Nonlinear optics can potentially support ultrafast self-processing of signals.

A variety of nonlinear optical signal-processing functions can be realized with similar fundamental building blocks [45.4–6]. Nonlinear optical elements and devices can be either integrated in photonic circuits [45.7] or used in a free-standing configuration [45.8]. Nonlinear optics can enable signal processing without the requirement for external electrical, mechanical, or thermal control [45.9]. The response time of properly designed nonlinear optical devices is limited fundamentally only by the nonlinear response time of the constituent materials [45.3, 10–12].

Photons do not interact with each other in vacuo. In order to perform nonlinear optical signal-processing operations the properties of a medium through which the light travels must be modified by the light itself. Optical signals then propagate differently as a result of their influence on the medium. Nonlinear optical signal-processing elements utilize the illumination-dependent real and imaginary parts of the index of refraction [45.9]. Depending on the material and spectral position, the real part of the refractive index and absorption of a given nonlinear material can either increase or decrease with increasing illumination.

A wide range of broadband and wavelength-selective nonlinear optical signal-processing devices has been proposed and demonstrated.

The most commonly studied nonlinear optical switching elements are nonlinear Fabry–Perot interferometers, nonlinear Mach–Zehnder modulators, nonlinear directional couplers, optical limiters, and nonlinear periodic structures.

A nonlinear Fabry–Perot interferometer consists of two mirrors separated by a nonlinear material. As the refractive index of the nonlinear material changes with an increased level of illumination, the effective path length of the resonator is altered. A nonlinear Fabry–Perot interferometer can be tuned out of, or into, its transmission resonance. When illuminated with the continuous-wave light, a nonlinear Fabry–Perot interferometer can exhibit optical bistability. Optical bistability is a phenomenon in which the instantaneous transmittance of the device depends both on the level of incident illumination and on the prior transmittance of the device. Such an element enables all-optical memory.

In a nonlinear Mach–Zehnder modulator and a nonlinear directional coupler, a part of the waveguide is made out of a nonlinear material. Changing the intensity of the incident light changes the effective path length experienced by the light. This, in turn, through phase interference, results in an illumination-dependent transmittance in a Mach–Zehnder modulator, and an illumination-dependent coupling in a nonlinear directional coupler.

A number of techniques use nonlinear properties of materials to obtain power-limiting, and associated with it, on–off switching. Such devices are based on total internal reflection [45.13], self-focusing [45.14], self-defocusing, two-photon absorption [45.15], or photorefractive beam fanning [45.16].

Nonlinear periodic structures combine the phenomena of nonlinear index change and distributed Bragg reflection. The intensity-dependent transmission and reflection properties of nonlinear periodic structures can be harnessed to yield various signal-processing functions. It has been demonstrated that nonlinear periodic structures can support optical switching and limiting [45.4–6, 17–20], optical bistability [45.8, 21–25], solitonic propagation of pulses [45.26, 27], and pulse compression [45.28].

45.1.3 The Approach Taken During this Survey of Nonlinear Optoelectronic Materials

There exist excellent texts that describe nonlinear optical processes and review the published properties of nonlinear materials [45.29–35]. This chapter will discuss the applicability of different material groups to nonlinear optical switching. Following the introduction of the concept of nonlinear refractive index and figures of merit in Sect. 45.2, the nonlinear properties of inorganic crystalline semiconductors (Sect. 45.3), organic materials (Sect. 45.4), nanocrystals (Sect. 45.5), and selected other materials (Sect. 45.6) will be reviewed and summarized. A critical review is given with a focus on figures of merit and processability.

45.2 Illumination-Dependent Refractive Index and Nonlinear Figures of Merit (FOM)

In a nonlinear optical medium intense light alters the real and imaginary components of the refractive index. The nonlinear response of the real part of the refractive index modifies the phase of propagating light, while the imaginary part describes the change in absorption.

This subsection will present the formalism used to describe how light affects the ultrafast and resonant changes in the nonlinear refractive index. The ultrafast nonlinear index changes take place in the spectral region where the material is nonabsorbing, while the resonant nonlinear index changes take place in the absorbing spectral region.

45.2.1 Ultrafast Response

Ultrafast nonlinear response is characterized by the instantaneous response, weak nonlinear index changes, and weak nonlinear absorption. The formalism that describes the ultrafast changes in the real and imaginary parts of the refractive index can be derived from the theory of nonlinear polarization.

The polarization $\boldsymbol{P}(r,\omega)$ of a material in the presence of an electric field $\boldsymbol{E}(r,\omega)$ at a frequency ω and position r is defined as

$$\boldsymbol{P}(r,\omega)=\epsilon_0\chi(r,\omega)\boldsymbol{E}(r,\omega)\,, \tag{45.1}$$

where ϵ_0 is the permittivity of free space and $\chi(r,\omega)$ is the dielectric susceptibility tensor. $\chi(r,\omega)$ is related to the index of refraction $n(\omega)$ by

$$\chi(r,\omega)=n^2(r,\omega)-1\,. \tag{45.2}$$

In a homogeneous nonlinear material $\chi(r,\omega)=\chi(\omega)$ but $\chi(\omega)$ is not constant with electric field and the influence of $\boldsymbol{E}(r,\omega)$ on $\boldsymbol{P}(r,\omega)$ is not linear. In this case it is customary to expand $\boldsymbol{P}(r,\omega)$ in a power series of $\boldsymbol{E}(r,\omega)$ [45.34]:

$$\begin{aligned}\boldsymbol{P}(r,\omega)=\epsilon_0\chi^{(1)}(\omega)\boldsymbol{E}(\omega)\\ +\epsilon_0\Bigg[D^{(2)}\sum_{j,k}\chi^{(2)}_{ijk}(-\omega_3;\omega_1,\omega_2)\\ \times\boldsymbol{E}_j(\omega_1)\boldsymbol{E}_k(\omega_2)\\ +D^{(3)}\sum_{jkl}\chi^{(3)}_{ijkl}(-\omega_4;\omega_1,\omega_2,\omega_3)\\ \times\boldsymbol{E}_j(\omega_1)\boldsymbol{E}_k(\omega_2)\boldsymbol{E}_l(\omega_3)\\ +\text{higher-order terms}\Bigg]\,,\end{aligned} \tag{45.3}$$

where $\chi^{(1)}$ is the linear susceptibility, while $\chi^{(2)}$ and $\chi^{(3)}$ are the coefficients of the second- and third-order nonlinear susceptibility. The coefficients $D^{(2)}$ and $D^{(3)}$ are defined as:

$$D^{(2)}=\begin{cases}1, & \text{for indistinguishable fields}\\ 2, & \text{for distinguishable fields}\end{cases} \tag{45.4}$$

and

$$D^{(3)}=\begin{cases}1, & \text{for all fields indistinguishable}\\ 2, & \text{for two fields indistinguishable}\\ 3, & \text{for all fields distinguishable}\end{cases} \tag{45.5}$$

In all known materials the higher-order components of the effective nonlinear susceptibility tensor $\chi(\omega)$ yield smaller contributions to the effective polarization than the preceding terms of the same parity. On the other hand, in the presence of strong electric field the terms designated as the *higher-order terms* in (45.3) [i. e. terms proportional to the powers of $\boldsymbol{E}(r,\omega)$ higher than four],

can be larger than the first three terms. However, the assumption of moderate intensities and the aim to illustrate the concept of nonlinear refractive index justifies retaining only the first three terms of (45.3) in the derivation that follows.

Nonlinear optical switching relies on nonlinear effects in which intense light changes the refractive index. Under such conditions there are no direct-current (DC) or low-frequency electro-optic effects present and the second term in (45.3) can be neglected. In addition all values of ω are degenerate. $\boldsymbol{P}(r, \omega)$ reduces to

$$\begin{aligned}\boldsymbol{P}(r,\omega) &= \epsilon_0[\chi^{(1)}(\omega)+\chi^{(3)}(\omega)\boldsymbol{E}(\omega)\boldsymbol{E}(\omega)]\boldsymbol{E}(\omega)\\ &= \epsilon_0\left[\chi^{(1)}(\omega)+\frac{2\chi^{(3)}(\omega)I}{\epsilon_0 n_0 c}\right]\boldsymbol{E}(\omega)\,, \end{aligned} \tag{45.6}$$

where I is the local intensity

$$I = \frac{\epsilon_0}{2} n_0 c |E(\omega)|^2\,, \tag{45.7}$$

and c is the speed of light in vacuum.

The first term in (45.6) represents the linear contribution to the polarization and the second term represents the nonlinear, intensity-dependent part. This intensity-dependent part gives rise to the nonlinear index of refraction fundamental to this work.

To obtain the direct expression for the nonlinear refractive index the effective susceptibility from (45.6) is substituted into (45.2) to yield

$$n^2 = 1+\chi^{(1)}+\frac{2\chi^{(3)}(\omega)I}{\epsilon_0 n_0 c}\,. \tag{45.8}$$

In order to relate directly this nonlinear part of polarization to the intensity-dependent part of the refractive index – a macroscopic measurable quantity – the effective index of refraction is expressed as

$$n = n_0 + n_2 I\,. \tag{45.9}$$

Taking the square of (45.9) and neglecting the terms proportional to I^2 under the assumption of weak relative nonlinearity $\left(n_2^2 I^2 \ll n_0 n_2 I \text{ and } n_2^2 I^2 \ll n_0^2\right)$ gives

$$n^2 = n_0^2 + 2 n_0 n_2 I\,. \tag{45.10}$$

Equating (45.8) and (45.10) gives an expression for n_2

$$n_2 = \frac{\chi^{(3)}}{\epsilon_0 n_0^2 c}\,, \tag{45.11}$$

where all the factors are in SI units.

In general, n_2 can have real (Re) and imaginary (Im) parts with $n_{2\,\mathrm{Re}}$ responsible for the nonlinear refraction and $n_{2\,\mathrm{Im}}$ responsible for the nonlinear absorption or gain. There are many conventions used to express the real and imaginary parts of the nonlinear refractive index. The approach used by researchers must always be determined prior to comparison with absolute numbers. However, in general it is safe to write

$$n_{2\,\mathrm{Re}} = \frac{K}{n_0^2}\,\mathrm{Re}\left(\chi^{(3)}\right) \tag{45.12}$$

and

$$n_{2\,\mathrm{Im}} = \frac{K}{n_0^2}\,\mathrm{Im}\left(\chi^{(3)}\right)\,, \tag{45.13}$$

where the constant K depends on the convention and units used [45.34].

In the rest of this chapter n_2 will be used to express the real part of the ultrafast nonlinear index of refraction, i. e. n_2 will be as used in (45.12).

In order to account for the imaginary component of the ultrafast nonlinear response in a commonly used way the following relationship is defined

$$\alpha = \alpha_0 + \beta I\,. \tag{45.14}$$

Equation (45.14) expresses the total absorption (α) in terms of its linear (α_0) and nonlinear (βI) contributions. β is the measurable, macroscopic quantity that will be used throughout this chapter to quantify the effects of the ultrafast imaginary nonlinear response.

45.2.2 Ultrafast Nonlinear Material Figures of Merit

A nonlinear material useful in a nonlinear optical signal-processing device must simultaneously satisfy the following conditions:

- The excitation time of the nonlinear effect must be less than the pulse width.
- The sum of the excitation and the relaxation times must be shorter than the pulse spacing.

In addition, an ultrafast nonlinear material must satisfy the following requirements:

- The effect of linear absorption must be weak compared to the effect of nonlinear refraction. *Stegeman* quantifies this condition in terms of the unitless figure of merit W [45.12]

$$W = \frac{|\Delta n|}{\alpha_0 \lambda} > 1\,, \tag{45.15}$$

where Δn is the induced change in the real part of the refractive index, α_0 is the linear absorption (expressed in units of inverse length) and λ

is the wavelength of light (with units of length). To facilitate consistent comparison between different nonlinear materials, Δn in (45.15) was assumed to be evaluated as the intensity approaches the saturation intensity, at which the rate of change of the refractive index drops noticeably below a linear dependence on intensity [45.12]. In general (45.15) can be used to quantify the nonlinear quality of a given material at any intensity, not only at the saturation.

- The effect of two-photon absorption must be weak compared to the effect of nonlinear refraction. This condition is quantified using the figure of merit T [45.12]

$$T = \frac{\beta_2 \lambda}{n_2} < 1 \,, \tag{45.16}$$

where β is the two-photon absorption coefficient from (45.14) (expressed in units of length/power).

The conditions (45.15) and (45.16) can be combined in terms of a single figure of merit F

$$F = \frac{|\Delta n|}{\alpha_{\text{eff}} \lambda} > 1 \,, \tag{45.17}$$

where α_{eff} is the effective absorption experienced by the sample at a given intensity. F can be used to quantify the quality of materials for signal processing with respect to nonlinear processes of any order rather than with respect to only third-order processes as in (45.16).

Condition (45.17) ensures that the nonlinear phase shift $\Delta\phi^{\text{NL}} = 2\pi \Delta n L/\lambda$, where L is the length of the material, reaches 2π before the intensity decays to $1/\text{e}$ of its input value as a result of the effective absorption. Phase shifts between 0.5π and 3.5π are required for most optical switching devices [45.12].

45.2.3 Resonant Response

The resonant response of a nonlinear material is the dominant nonlinear effect in the linearly absorbing spectral region. A different formalism than that presented in Sects. 45.2.1 and 45.2.2 is used to describe the resonant changes in the real and imaginary parts of the refractive index.

Illumination with light which is resonant with the material results in the direct absorption of the incoming photons, generating excited states and giving rise to a decrease in the effective absorption. If the relaxation time of the excited states is longer than the length of the pulse, the resonant effect is proportional to the fluence, rather than to the intensity of the incident ultrafast pulse. This saturation of the absorption is described by the following expression for the effective absorption α_{eff} [45.35]

$$\alpha_{\text{eff}} = \frac{\alpha_0'}{1 + \frac{P}{P_{\text{sat}}}} + \alpha_{\text{u}} \,. \tag{45.18}$$

where α_{u} is the unsaturable absorption, $P = \int_0^t I(t')\,\text{d}t'$ is the incident fluence and P_{sat} is the saturation fluence at which the effective absorption decreases to half of its initial value $\alpha_0 = \alpha_0' + \alpha_{\text{u}}$. P accounts for the cumulative (up to the duration of the pulse) character of the resonant nonlinear response.

The saturation of absorption is accompanied by a change in the real part of the refractive index [45.35]

$$\Delta n = \frac{n_2' P}{1 + \frac{P}{P_{\text{sat}}}} \,. \tag{45.19}$$

n_2' describes the strength of the real part of the resonant nonlinear refractive index.

In this chapter, nonresonant and resonant phenomena are considered. The parameters n_2 and β from Sect. 45.2.1 are used to quantify the ultrafast response and Δn and $\Delta\alpha$ from Sect. 45.2.1 are used to describe the resonant response.

45.2.4 Resonant Nonlinear Material Figures of Merit

Figures of merit for the nonresonant response have been defined in Sect. 45.2.2. This section will introduce resonant figures of merit that account for the nonlinear phase shift that accumulates over the duration of a pulse.

For illustrative purposes, first-order approximations to (45.18) and (45.19) of the form $\Delta n(t) = \int_0^t n_2' I(t')\,\text{d}t'$ and $\alpha_{\text{eff}}(t) = \alpha_0$ are considered under the assumption $P \ll P_{\text{sat}}$. A resonant nonlinear material is assumed to be illuminated with a square pulse of the form:

$$I(t) = \begin{cases} I_0, & \text{if } 0 < t < \tau_{\text{p}} \\ 0, & \text{if } t < \tau_{\text{p}} \,. \end{cases} \tag{45.20}$$

In analogy to (45.17) a time-averaged nonlinear figure of merit is defined for the resonant response

$$\langle F \rangle = \frac{|\langle \Delta n \rangle|}{\langle \alpha \rangle \lambda} \,. \tag{45.21}$$

The time-averaged nonlinear index change is

$$\langle \Delta n \rangle = \frac{1}{\tau_p} \int_0^{\tau_p} \left[\int_0^t n_2' I(t') \, dt' \right] dt$$
$$= \frac{n_2' P_{\text{total}}}{2} = \frac{\left| \Delta n_{\text{peak}}^{\text{ultrafast}} \right|}{2} , \quad (45.22)$$

where P_{total} is the total fluence of the pulse $P_{\text{total}} = \int_0^{\tau_p} I(t') \, dt' = I_0 \tau_p$. The time-averaged absorption is $\langle \alpha \rangle = \alpha_0$. For the case considered, the figure of merit (45.21) becomes:

$$\langle F \rangle = \frac{|\Delta n_{\text{peak}}|}{2 \alpha_0 \lambda} , \quad (45.23)$$

which is half of the ultrafast figure of merit. For simplicity, (45.17) will be used throughout this chapter for both resonant and ultrafast response.

45.3 Bulk and Multi-Quantum-Well (MQW) Inorganic Crystalline Semiconductors

The illumination-dependent refractive and absorptive nonlinear properties of inorganic crystalline semiconductors have been studied comprehensively. Since semiconductors are at the heart of the electronics industry, semiconductor micro- and nanofabrication techniques are well established. This enables the preparation of high-quality nonlinear samples and devices. The ability to change the composition of semiconductor compounds allows the tuning of the electronic band gap over the visible and infrared spectral ranges. The spectral position of the band gap, in turn, tunes the nonlinear properties.

When a semiconductor is illuminated with light at a frequency within the absorbing region, the dominant nonlinear effect relies on the presence of linear absorption. Upon absorption of the incident light, the electrons undergo a transition from the valence band to the conduction band, saturating the absorption. This band-filling effect is accompanied by a very large change in the real part of the refractive index.

In a nonresonant nonlinear process no single-photon absorption takes place. Under illumination with intense light the electronic clouds of the constituent atoms are distorted, changing the refractive index of the material. Associated with this is a multiphoton absorption process which takes place when the sum of the photon energies is larger than the band-gap energy. This effect changes the absorption characteristics of the material. Both the real and imaginary parts of ultrafast nonlinear index change, given their connection through the nonlinear Kramers–Kronig relations.

In addition, when subjected to an intense continuous wave or a high-repetition-rate pulsed illumination, the temperature of the absorbing materials, including semiconductors, increases. This in turn changes the refractive index. Thermal effects have relaxation times as long as milliseconds and are not useful in processing trains of closely spaced pulses.

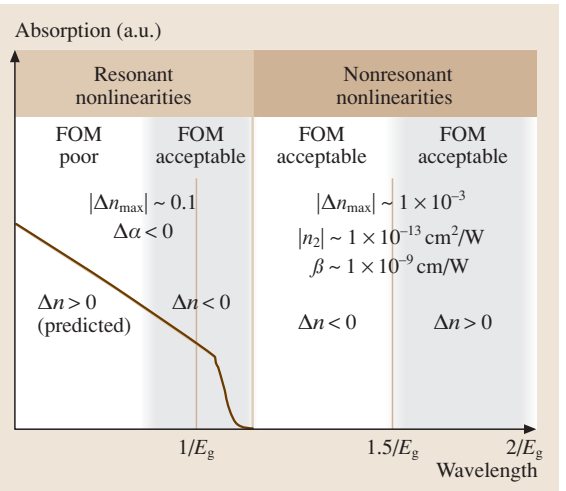

Fig. 45.1 Trends in the nonlinear response of bulk semiconductors

Figure 45.1 shows typical trends in the nonthermal nonlinear response of bulk inorganic crystalline semiconductor material under picosecond, low-repetition-rate illumination.

45.3.1 Resonant Nonlinearities

The two most important characteristics of the resonant nonlinear response are saturation of absorption and large nonlinear index change [45.36–38]. The relaxation of resonant nonlinear effects in semiconductors is not instantaneous. As long as the duration of the incident pulse is shorter than the relaxation time of the material, the magnitude of a nonlinear resonant response

is proportional to the fluence, rather than to the intensity of the incident pulse. The relatively long relaxation time of nonlinear effects in bulk and multi-quantum-well (MQW) inorganic crystalline semiconductors (from hundreds of picoseconds to tens of nanoseconds) is often used as an argument against using resonant nonlinearities. However, established techniques such as low-temperature growth and doping can reduce the relaxation time down to tens of picosecond [45.39, 40].

The phenomenon of saturation of absorption ($\Delta\alpha < 0$) translates into absorption that decreases with increasing incident fluence. Resonant figures of merit of semiconductors are acceptable near the band edge and become worse at lower wavelengths. Such behavior is due to a stronger, lower-threshold saturation of absorption around the band edge.

Nonlinear index change is negative around the band edge and has been predicted to be positive at wavelengths lower than those corresponding to the first heavy-hole and light-hole excitonic peaks.

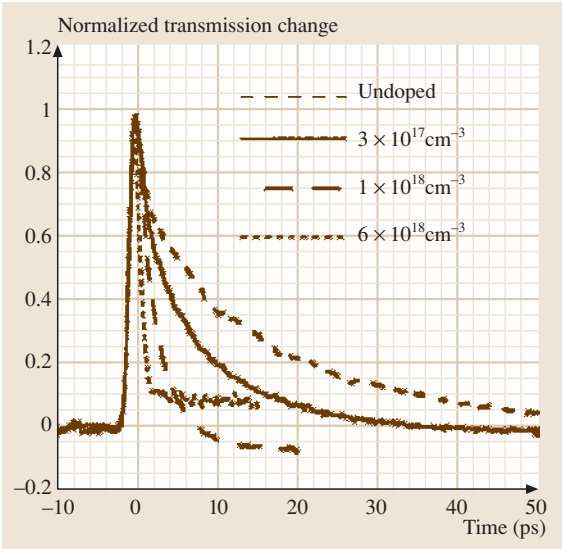

Fig. 45.2 Results of the pump-probe measurements illustrating the time-resolved change in transmission for He-InGaAsP samples with different Be doping concentrations. (After [45.41] with permission)

Resonant Nonlinearities in Bulk Semiconductors

In 1991 *Gupta* et al. measured the time of nonlinear response of GaAs grown at low temperatures (LT-GaAs) [45.42]. Changes in reflectivity were monitored during a pump-probe experiment at 620 nm. Relaxation times of several 2-μm-thick samples grown at temperatures ranging between 190 °C and 400 °C were measured. A decrease in the decay time to 0.4 ps was recorded with decreasing growth temperatures. This short relaxation time is drastically lower than the typical value of nanoseconds for unannealed GaAs [45.42].

In 1993 *Harmon* et al. studied the dependence of the nonlinear relaxation time in LT-GaAs on annealing temperatures. A decrease in the relaxation time down to sub-picosecond values was observed with decreasing annealing temperatures [45.43].

In a number of papers published between 1994 and 1998, the group of Smith, Othonos, Benjamin, and Loka reported on a series of comprehensive experiments carried out on various LT-GaAs samples grown using molecular beam epitaxy (MBE). The dependence of the magnitude and the response time of nonlinear effects on the growth and annealing temperatures was studied. Very large negative nonlinear index changes were measured ($\Delta n_{max} = -0.13$) accompanied by a strong saturation of absorption [45.44]. The relaxation time was measured to decrease to a few picoseconds for samples grown at 500 °C [45.45]. The pump-probe measurements were carried out in the band-edge region at wavelengths of 870–890 nm. The decreased response time was attributed to the fast decay of excited carriers to mid-gap states. These states are an effect of the LT growth [45.40].

In subsequent years another group of researchers studied the strength and dynamics of intensity-dependent response in InGaAsP doped with Be grown with He-plasma-assisted MBE. As illustrated in Fig. 45.2, sub-picosecond relaxation times were obtained [45.41]. The rapid decay was explained by a short lifetime of excited states due to the existence of mid-gap He and He–Be trap states. Again, large negative changes in the real part of the refractive index and strong saturation of absorption were observed [45.39].

Resonant Nonlinearities in Semiconductor Multi-Quantum-Wells

The nonlinear properties of semiconductor multi-quantum-wells (MQWs) are similar to those of bulk semiconductors [45.38, 46, 47]. The nonlinear response in MQWs around the band edge is stronger and begins at lower fluences than in bulk materials.

Compared with bulk semiconductors, semiconductor MQWs offer an additional degree of freedom in selecting their nonlinear properties. The effective electronic band gap of a given semiconductor MQW structure, and hence the dispersion of real and imaginary

parts of its linear and nonlinear refractive index, are influenced by two factors: the choice of the compositions of the constituent compounds and the well-to-barrier thickness ratio.

In 1982 *Miller* et al. reported on the measurements of resonant nonlinear properties of semiconductor MQWs. A very strong absorption saturation was noticed around the first excitonic peak in GaAs/AlGaAs MQWs. Based on these results a large refractive nonlinearity was deduced from the nonlinear Kramers–Kronig relation [45.48]. A theoretical paper followed, explaining the dynamics of transient excitonic nonlinearities [45.49]. A 20-ns excited-carrier relaxation time was predicted.

In 1986 *Lee* et al. measured the nonlinear saturation of the absorption of bulk GaAs and 29.9-nm GaAs/AlGaAs wells grown by molecular beam epitaxy. The measurement was performed using a monochromatic pump and a broadband probe over a 40-nm spectral range near the MQW band edge. Using the nonlinear Kramers–Kronig relation, large index changes of both signs were predicted. In MQWs, absorptive and refractive nonlinearities were enhanced compared to bulk GaAs. Index changes ranging from $\Delta n = -0.06$ to $\Delta n = 0.03$ were predicted in the samples analyzed [45.50].

This report was followed in 1988 by a study of nonlinearities around the band edge carried out by the same research group [45.38]. The response of bulk GaAs was compared with that of three sets of GaAs/AlGaAs MQWs, with well thicknesses of 7.6 nm, 15.2 nm and 29.9 nm. Again, a strong saturation of absorption was measured and nonlinear index changes of both signs were predicted from the nonlinear Kramers–Kronig relation [45.51]. The magnitude of the change in the real part of the refractive index was predicted to increase with decreasing well size. The sign of the refractive nonlinearity changed at wavelengths slightly shorter than that corresponding to the first excitonic peak [45.38].

Since 1988 many results of research on the nonlinear properties of GaAs/AlGaAs MQWs have been reported by *Garmire* et al. In a series of papers, the saturation of absorption was studied in GaAs/AlGaAs MQWs grown by metalorganic chemical vapor deposition epitaxy. The nonlinear Kramers–Kronig relation was used to predict the associated change in the real part of the refractive index. Figure 45.3 shows the predicted enhancement of nonlinearity with decreasing well size and the change of sign near the excitonic peak. Attempts were made to use the illumination-dependent shift of Fabry–Perot fringes to estimate directly the negative nonlinear index change along the band edge. However, this approach was admitted to yield significant errors, with the Fabry–Perot technique sometimes giving a value of Δn at twice the magnitude predicted

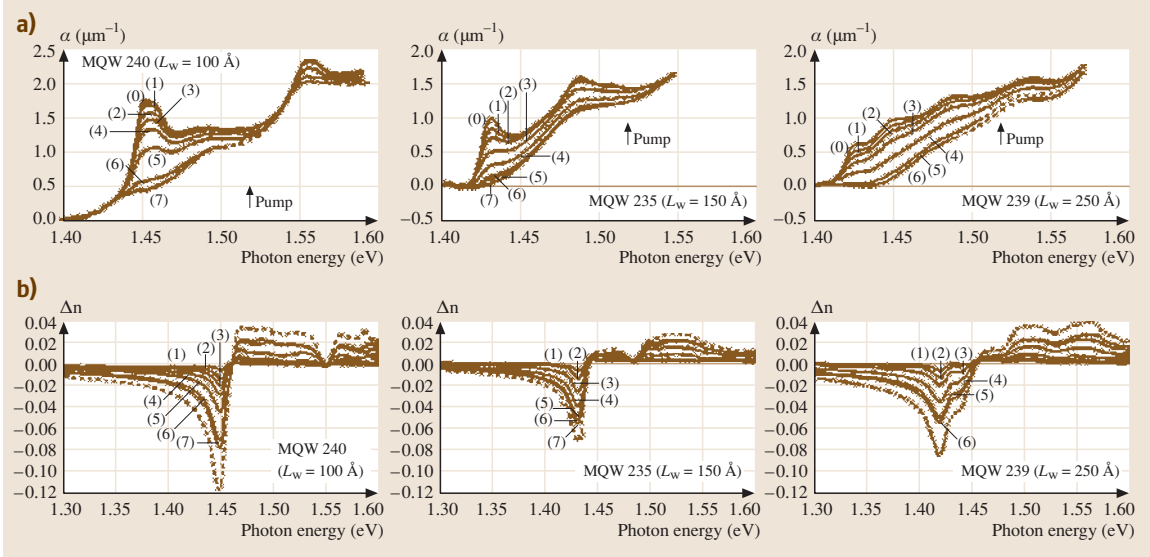

Fig. 45.3a,b Spectra of GaAs/AlGaAs MQWs of three different well widths, measured at various incident intensities by pulsed pump at 1.52 eV: **(a)** absorption coefficient α; **(b)** the change in the real part of the refractive index Δn. (After [45.46] with permission)

from the Kramers–Kronig relation [45.46]. In 1987 *Fox* et al. reported nonlinear measurements around the band edge of bulk GaInAs [45.52] and GaInAs/InP MQWs near wavelengths of 1.6 μm [45.53]. Full saturation of absorption was observed. The nonlinear index changes deduced from the nonlinear Kramers–Kronig relation were slightly larger than that observed in GaAs [45.35].

Recently *Brzozowski* et al. published results of direct picosecond measurements of nonlinear refractive-index change and nonlinear absorption in $In_{0.530}Al_{0.141}Ga_{0.329}As/In_{0.530}Ga_{0.470}As$ multi-quantum-wells in the range 1480–1550 nm. Large low-threshold nonlinear index changes were found: Δn of up to 0.14 with a figure of merit of 1.38 at a fluence of 116 $\mu J/cm^2$. The figure of merit F was greater than unity over much of the spectrum. The results are summarized in Fig. 45.4.

In 1996 *Judawlikis* et al. reported the decreased nonlinear relaxation time in LT-grown Be-doped InGaAs/InAlAs MQWs. Nonlinear relaxation times of a few tens of picoseconds were observed in a pump-probe experiment near the band edge. The nonlinear change in the real part of the refractive index was not reported [45.56].

A different approach to decrease the response times of band-edge nonlinearities of semiconductor MQWs was taken by the groups of White, Sibbet, and Adams. An electric current was applied to active InGaAsP/InP waveguides and the nonlinear optical response under electrical bias was studied. It was found that under a forward bias the refractive nonlinear response was quenched. Under a reverse bias the nonlinear response was slightly reduced, but the initially long recovery time was reduced to 50 ps [45.57] and 18 ps in subsequent experiments [45.58]. Further, it was found that, when the waveguide was biased at transparency, the nonlinear coefficients of the semiconductor MQW waveguides were $n_2 = 4\times10^{-11}\,cm^2/W$ and $\beta = 4\times10^{-9}\,cm/W$, giving a combined figure of merit of $F = 7$ [45.59]. In all measurements the negative nonlinear index changes were measured to have magnitude smaller than $|\Delta n| < 0.001$ [45.60].

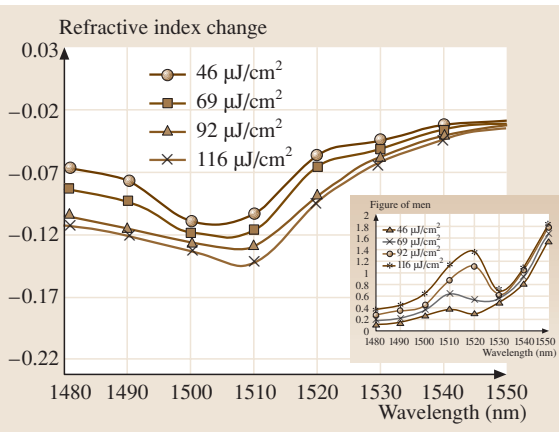

Fig. 45.4 Nonlinear index changes of 121 10-nm $In_{0.530}Al_{0.141}Ga_{0.329}As$ barriers and 120 5-nm $In_{0.530}Ga_{0.470}As$ wells grown on S-doped 001 InP wafer substrate. The *inset* shows the corresponding figures of merit. (After [45.54, 55])

45.3.2 Nonresonant Nonlinearities in Inorganic Crystalline Semiconductors

Nonresonant nonlinearities are not triggered by direct electronic transitions due to single photons. Much weaker effects of distortion of electronic clouds and multi-photon absorption are responsible for nonresonant nonlinear response. Maximum nonresonant nonlinear index changes are of the order $|\Delta n_{max}| \approx 1\times10^{-3}$. Since in certain spectral regions a typical nonresonant Kerr coefficient is $n_2 \approx 1\times10^{-13}\,cm^2/W$, the linear absorption is around $5\,cm^{-1}$, and the corresponding two-photon absorption coefficient is $\beta \approx 1\times10^{-9}\,cm/W$, the figures of merit associated with nonresonant semiconductor nonlinearities can be acceptable.

The biggest advantage of nonresonant semiconductor nonlinearities is their sub-picosecond response time. The sum of the rise and relaxation times of nonresonant nonlinearity has been argued to be comparable to the orbital period of an electron in its motion about the nucleus, estimated to be around 10^{-16} s [45.29].

Depending on the spectral region, bulk and MQW inorganic crystalline semiconductors may exhibit either positive or negative refractive nonresonant nonlinearities. Under illumination with sub-nanosecond pulses at low repetition rates, the nonlinear index change is negative for wavelengths up to $1.5ch/E_g$, where ch/E_g is the wavelength corresponding to the band gap, and h is Planck's constant. Δn is positive for wavelengths longer than $1.5ch/E_g$ [45.37, 61]. In MQWs the spectral position of the sign change in Δn depends on the nanostructure of MQWs [45.62]. In 1993 *Shaw* and *Jaros* predicted through theory the dispersion of refractive nonlinearity in semiconductor MQWs and superlattices. They found that in MQWs the proximity of the spectral position of the Δn sign change to the band edge increases with increasing quantum confinement [45.62].

Under nonresonant illumination with pulses longer than one nanosecond, there is no sign change in the refractive nonlinearity. The negative nonlinearity originating from two-photon absorption-induced free-carrier effects is much stronger than any positive third-order refractive effects at moderate and high intensities for $hc/E_g < \lambda < 2hc/E_g$. Consequently, the measured Δn is always negative in this spectral range [45.63].

The group of Sheik-Bahae and Van Stryland has authored several reports on the prediction of the spectral dependence of nonresonant nonlinearities in semiconductors. In 1985 *Van Stryland* et al. predicted trends in the absorptive ultrafast nonlinear response of semiconductors. An equation for the two-photon absorption below the band gap was derived and compared with experimental values. Dispersion of two-photon absorption is expected to mimic the dispersion of linear absorption; i. e. two-photon absorption is strong and relatively flat from the band gap to almost the midpoint of the band gap, at which point it goes to zero. Good agreement was obtained between experiment and theory for photon energies not in the vicinity of the band gap, with two-photon absorption coefficients of various semiconductors ranging from $\beta = 3\times10^{-9}$ cm/W to $\beta = 25\times10^{-9}$ cm/W [45.36].

In the ensuing years the same research group reported theory describing the spectral dependence of the real part of the ultrafast nonlinearity and compared it with experiments. The results are shown in Fig. 45.5. The magnitude of n_2 is largest near the photon energy corresponding to half of the band gap. Since, for wavelengths longer than that corresponding to half the band gap, two-photon absorption vanishes, large figures of merit can be expected in these spectral region. In addition, n_2 was predicted to be positive for wavelengths longer than that corresponding to $0.75E_g$, and negative between $0.75E_g$ and E_g [45.37, 64]. A large discrepancy between theoretical and experimental results was observed near the band gap, where the theory drastically underestimated the strength of the refractive nonlinearity.

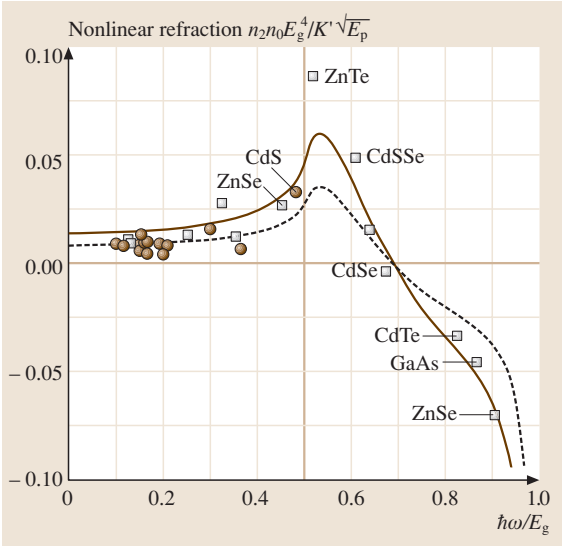

Fig. 45.5 Dispersion of the refractive nonlinearity of inorganic crystalline semiconductors in the transparent region. The *points* correspond to the experimental data explained in [45.37], while the *lines* are a fit to the theory. (After [45.37])

45.4 Organic Materials

Organic materials constitute another class of promising nonlinear materials. Organic materials exhibit significant nonlinearities across the visible and infrared spectral regions [45.65]. They are readily processable into thin-film waveguide structures [45.33, 66] and in general do not rely on a high degree of perfection in ordering or purity to manifest their desired properties. The molecules that make up organic materials provide a tremendous range of structural, conformational, and orientational degrees of freedom for exploration with the aid of novel synthetic chemistry. This permits flexible modification and optimization of linear and nonlinear properties [45.33].

As is the case with semiconductor nonlinearities, the nonlinear response of organic materials can be divided into resonant and nonresonant parts, occurring in the absorbing and transparent regions, respectively. The resonant nonlinearities are a result of a single-photon absorption, while the nonresonant nonlinearities arise as a result of perturbations of electronic clouds and multi-photon absorption.

Depending on the structure of the constituent molecules, organic materials may exhibit many absorption resonances and hence many spectral areas of different strength and sign of nonlinear response. Phenomena such as molecular reorientation and pho-

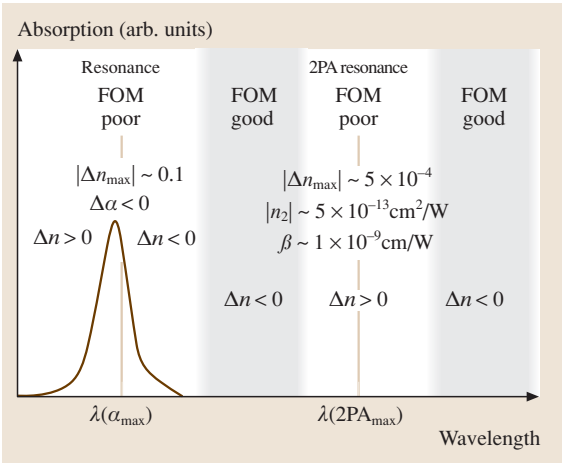

Fig. 45.6 Typical trends in the nonlinear response of organic materials with one absorption resonance

toisomerization, which are often found in organic materials, make the picture even more complex.

Some organic materials, such as most nonlinear dyes, have only one absorption resonance, which permits the qualitative prediction of their nonlinear response in the visible and near-infrared regions. Fig. 45.6 shows the nonlinear response of a typical nonlinear organic material with one absorption resonance.

In general, the figures of merit of organic materials in the absorbing region are poor. However, molecular effects such as trans–cis photoisomerization strongly increase the nonlinear index change along the absorption edge. The magnitudes of ultrafast nonlinearities and associated figures of merit of organic materials are comparable to those of inorganic crystalline semiconductors.

45.4.1 Resonant Nonlinear Response of Organic Materials

Since 1998 *Rangel* and *Rojo* et al. have reported resonant nonlinear properties of various organic compounds. The nonlinear refraction and absorption effects were reported in and near the absorbing regions of: solid-state PMMA samples doped with nonlinear azobenzene dye Disperse Red 1 [45.67], polydiacetylene microcrystals in aqueous suspension [45.68], cyclohexane suspensions of vanadium-oxide phthalocyanine microcrystals [45.69, 70], solid-state samples of plythiophene/selenophene copolymer [45.71], and a chloroform solution of triazole-quinone derivation [45.72].

PMMA films doped with Disperse Red 1 (10% molar concentration) have been shown to exhibit large, low-threshold nonlinear index changes and saturation of absorption as a result of optically induced structural changes in the middle and near the edge of the absorption resonance at 490 nm [45.67]. The nonlinear index changes associated with this photochemical phenomenon, called *trans–cis photoisomerization* have exceeded 0.1 in the spectral region $\lambda < 590$ nm. As illustrated in Fig. 45.7 [45.67], light near the main absorption resonance causes the azobenzene molecule to change from the *trans* to the *cis* configuration. During this process, the distance between the two carbons from which the acceptor and donor groups extend reduces from about 9.0 Å to 5.5 Å. This results in a drastic reduction in the molecule's dipole moment, which reduces the material's polarizability, providing a large negative nonlinearity with nonlinear index changes reaching $\Delta n_{max} = 0.12$ at 560 nm under illumination with 20-ps pulses at a repetition rate of 10 Hz [45.67]. The figures of merit calculated according to (45.17) did not exceed 0.42 over the spectral range studied.

The refractive and absorptive nonlinear properties of polydiacetylene microcrystals in aqueous solution have been analyzed across their absorbing and near resonance regions 500–800 nm [45.68] with the same system as in [45.67]. As shown in Fig. 45.8, both negative and pos-

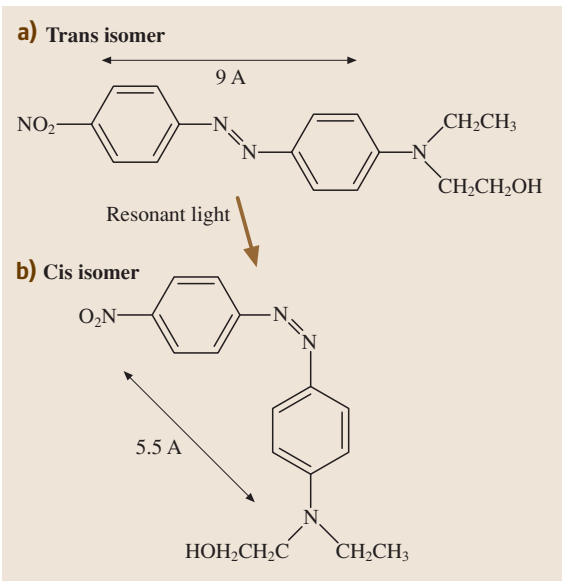

Fig. 45.7 Chemical structure of the azobenzene dye Disperse Red 1 undergoing trans–cis photoisomerization. Following resonant absorption, the azobenzene molecule changes its configuration, resulting in a decreased dipole moment. (After [45.67] with permission)

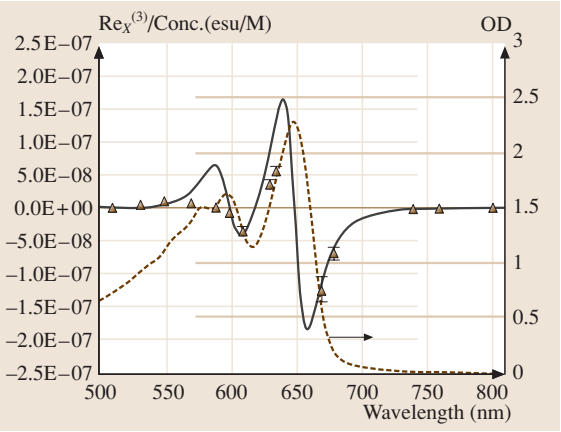

Fig. 45.8 $\chi^{(3)}$ and linear absorbance as a function of wavelength for 100-nm polydiacetylene microcrystals. (After [45.68])

itive nonlinear index changes were observed, depending on the spectral position relative to one of the two absorption resonances in the visible region. Saturation of absorption was observed across the entire absorbing region. A three-level model was developed to explain the data. Because of the low concentration of microcrystals in water, the absolute values of the nonlinear index change did not exceed 2×10^{-4}, while the figures of merit stayed below 0.26.

Cyclohexane suspensions of vanadium-oxide phthalocyanine microcrystals have also been characterized around its main absorption resonance peak in the spectral range 600–680 nm [45.69, 70]. Similarly to the nonlinear response of polydiacetylene microcrystals, both signs of refractive nonlinearity were observed, with the sign of the nonlinearity tracing the derivative of the linear absorption. Solid-state samples of plythiophene/selenophene copolymer were analyzed near the absorbing region and have shown only negative nonlinearity [45.71]. These results contradicted the predictions from nonlinear Kramers–Kronig transformation, which predicts positive nonlinearity in the spectral region where absorption increases with wavelength. The origins of this discrepancy were not understood.

In 1997 *Demenicis* et al. reported on the measurements of nonlinear properties of poly(3-hexadecylthiophene) in a chloroform solution around the absorption edge of 532 nm with 70-ps pulses at a repetition rate of 5 Hz [45.73]. Saturation of absorption and negative nonlinearity was observed. The saturation intensity decreased with increasing concentration, while the nonlinear absorption and nonlinear refraction at low intensity increased linearly. Figures of merit were not given.

45.4.2 Nonresonant Nonlinear Response of Organic Materials

In the 1970s it was predicted from theory and experimentally demonstrated that the conjugation of organic molecules results in a strong electronic delocalization and an associated large third-order nonlinearity in the transparent spectral region. This region extends between the main absorption peak due to the band-to-band transition and the first of the vibronic modes of the conjugated chain [45.74, 75]. It was demonstrated that the solid-state polymerization of organic monomers results in $\chi^{(3)}$ values comparable to these observed in inorganic crystalline semiconductors. Numerous studies followed that concentrated on the determination of the length and bond order of the conjugation chain, and acceptor and donor strengths that yield the strongest nonlinear response. *Marder* et al. provide an excellent summary of the field of nonresonant nonlinear response of organic molecules in [45.76].

Single-crystal polydiacetylene para-toluene sulphonates (PTS) have received special attention among the organic nonlinear compounds. In 1994 *Lawrence* et al. reported that at 1600 nm PTS has a large nonlinear refractive index of $n_2 = 2.2\times10^{-12}\,\mathrm{cm^2/W}$ [45.77]. Since linear absorption of PTS is very low at this wavelength, and two-photon absorption was below experimental sensitivity ($\beta < 0.5\,\mathrm{cm/GW}$), and very large figures of merit were predicted with W exceeding unity for incident intensities as low as $20\,\mathrm{MW/cm^2}$, and T never exceeding 0.1. A report followed in which *Lawrence* et al. showed measured two-photon absorption and nonlinear refraction values of PTS in the spectral range 800–1600 nm [45.78]. The two-photon-absorption coefficient varied in the range 0–700 cm/GW while the measured n_2 coefficient was between $n_2 = -2.2\times10^{-12}\,\mathrm{cm^2/W}$ and $n_2 = 4.3\times10^{-12}\,\mathrm{cm^2/W}$. In 2000 and 2003 *Yoshino* et al. published two reports where the influence of three- and four-photon absorption on the nonlinear response was studied in the near-infrared region [45.79, 80]. For wavelengths of 1600–2200 nm the nonlinear refraction coefficient n_2 was around $n_2 = 5\times10^{-13}\,\mathrm{cm^2/W}$ while nonlinear absorption was dominated by three- and four-photon effects.

Although PTS exhibits nonlinear refractive-index changes and figures of merit that are very large for non-

linear material in the transparent region, PTS suffers from low processability – as a single-crystal it cannot be easily processed into desired shapes.

Third-order nonresonant nonlinear properties of fullerene organic compounds have also attracted significant attention [45.81, 82]. Recently *Chen* et al. reported nonlinear coefficients and figures of merit of high-quality polyurethane films heavily loaded with (60)fullerene (C_{60}) [45.83]. Nonlinear refractive coefficients in excess of 10^{-12} cm^2/W were reported in the wavelength range 1150–1600 nm with very good figures of merit.

45.5 Nanocrystals

Nanoscale quantum-confined inorganic crystalline semiconductors represent an interesting group of nonlinear materials [45.84]. The size of such quantum dots is less than the bulk radii of excitons, holes, and electrons in a given semiconductor. As in the case of semiconductor MQWs, this results in quantum confinement of carriers. In a nanocrystal, this takes place in all three dimensions [45.85, 86]. Quantized energy levels make nanocrystals an artificial analogue of noninteracting atoms in a gas, raising the possibility of explaining the nonlinear processes by adopting the models of atomic physics.

To allow processability nanocrystals are usually embedded in either solid or liquid, organic or glass, optically linear hosts. Nanocrystal material systems are thus hybrids of semiconducting and insulating materials and combine interesting properties from both material groups. As in the case of semiconductor MQWs, the composition and size of quantum dots determines the energy of the electronic transitions. This allows spectral tunability of absorption features and nonlinear properties over the entire visible and infrared spectrum. On the other hand, the organic or glass host permits flexible fabrication of samples, waveguides, and other integrated components using polymer photonics technologies [45.87].

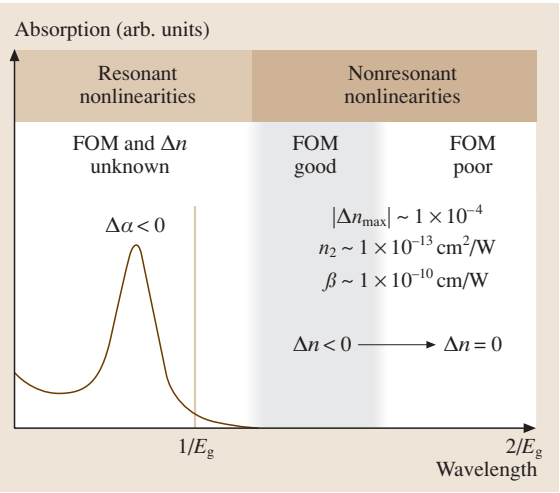

Fig. 45.9 Trends in the picosecond nonlinear response of inorganic semiconductor nanocrystals

Figure 45.9 shows the properties of a typical resonant and nonresonant nonlinear response of strongly confined semiconductor nanocrystal composites. The data presented in this figure are based on the published theoretical predictions and experimental reports.

The finite number of allowed lower electronic levels leads to more pronounced excitonic features and resonant nonlinearities, which take place at lower fluences than in bulk or MQW inorganic crystalline semiconductors [45.88].

Similarly to the nonlinear response of bulk and MQW semiconductors, the resonant nonlinear response of nanocrystals is characterized by the saturation of absorption and an associated large change in the real part of the refractive index.

Saturation of absorption in strongly confined PbS quantum-dot glasses was measured in the spectral range 1.2–1.3 μm [45.89], covering the spectral position of the valley between the first and second excitonic peaks in the 6.6-nm-diameter sample studied. This material system was used as a passive saturable absorber in the production of 4.6-ps pulses via mode-locking around a wavelength of 1.3 μm [45.89]. The report was followed by studies of saturation of absorption dynamics in quantum dots of various sizes at a wavelength of 1.3 μm. This wavelength covered spectral regions ranging from the first to second electronic transitions, depending on the size of nanocrystals. The saturation energy and nonlinear decay times at a given wavelength were found to decrease with increasing size of nanocrystals [45.90]. Values for the refractive nonlinearity were not reported.

Saturation of absorption in PbS quantum-dot-doped glasses was also studied under illumination with 70-ps and 15-ns pulses 1.06 μm [45.91]. The

nanocrystals analyzed had mean radii of 1.7–2.7 nm, resulting in excitonic peaks at wavelengths in the range 1.0–1.5 μm. The saturation intensity of the for the samples analyzed was found to be 2.3 MW/cm^2 and the relaxation time was measured to be 23 ± 2 ps.

Lu et al. measured the resonant nonlinear refractive properties of strongly confined 3.3-nm-diameter PbS nanocrystals in polymeric coatings over the spectral range 580–630 nm. This spectral range corresponds to the wavelengths around the first excitonic peak. The degenerate four-wave-mixing technique was used to measure the nonlinear susceptibility of nanocrystals near the photon energy of the first electronic transition at 595 nm. The values were found to fall in the range $\chi^{(3)} = 1 \times 10^{-6} - 1 \times 10^{-5}$ esu. Combined with the 50 kW/cm^2 intensity used in the experiment these values of $\chi^{(3)}$ suggest maximum nonlinear index changes of $\Delta n \approx 0.013$. No data on saturation of the absorption were reported.

The nonresonant nonlinear response of nanocrystals shows different dispersion characteristics than that of any other material group. Under illumination with picosecond pulses, the nonresonant third-order nonlinearity is negative for photon energies between half the band gap and the band gap [45.92]. The magnitude of the third-order nonlinear response increases with proximity to the band gap, and disappears entirely near the half-band-gap energy. Such a response is in contrast to the Δn sign change between absorption and two-photon absorption resonances as observed in bulk semiconductors and organic materials. However, similarly to the nonresonant response of bulk semiconductors, the sign of the nonresonant refractive nonlinearity in the semiconductor-doped glasses in some spectral regions depends on the duration of the pulses used to measure the nonlinear effect. For pulses shorter than 1 ps the contribution of third-order positive refractive effects is comparable to that of the negative free-carrier absorption nonlinearities of the fifth order. Consequently, the measured Δn can be positive [45.63].

In 2000 and 2001 *Liu* et al. published several reports on measurements of the ultrafast nonlinearities of PbS nanoparticles, and PbS-coated CdS nanocomposites [45.93–95]. Surprisingly large refractive nonlinear indices of refraction up to -5×10^{-12} cm^2/W and unmeasurable nonlinear absorption were observed in surface modified polymer–PbS composites at moderate concentrations of 1.9×10^{-3} mol/l. This large refractive nonlinearities were attributed to the surface recombination owing to the high surface-to-volume ratio of PbS nanoparticles.

45.6 Other Nonlinear Materials

Metallic nanocomposites and cascaded second-order materials are two other promising groups of nonlinear materials. Metalorganic nanocomposites are made out of metallic quantum dots embedded in organic or glass hosts. Resonant nonlinear properties of copper [45.96] and silver nanoparticles [45.97, 98] embedded in a glass host were measured using degenerate four-wave-mixing experiments at visible wavelengths. The nonlinear coefficients and figures of merit of the metallic nanocrystals characterized were similar to those of semiconductor nanocrystals and reached a maximum near the plasma-frequency absorption peak.

It has been argued that metallic nanoparticles can potentially exhibit stronger nonlinear effects than other material systems [45.99]. This is associated with local field effects that enhance nonlinear response of the composite systems if the refractive index of the nonlinear constituent is lower than that of the linear host. Such a scenario can be realized in metallic nanoparticle–glass composites, since around the spectral positions of the plasma resonance the refractive index of metals can be lower than 1.

Cascaded nonlinear materials are made out of materials with second-order nonlinear properties. An appropriate design of such structures design results in a net accumulated phase shift for the illumination at a fundamental optical frequency at the end of a cascaded system. Cascaded material system acts as an effective third-order nonlinear material [45.100–102].

45.7 Conclusions

Following the preceding review, this section will summarize the major conclusions, as well as the missing pieces, of the published literature on nonlinear optical materials.

Bulk and MQW semiconductors have been demonstrated to exhibit low-threshold saturation of absorption near the band edge. The spectral position of the band edge can be tuned over the entire visible and near-infrared spectrum. It has been predicted from the nonlinear Kramers–Kronig relation, and has been measured directly in isolated cases, that the band-edge saturation of absorption results in large changes of the real part of refractive index.

In the regions of transparency, semiconductors exhibit weak nonlinear refractive effects of both signs. The nonresonant effects can be accompanied by two-photon absorption. Depending on the spectral position, the nonresonant nonlinear response of semiconductors can be characterized by good figures of merit.

Semiconductor nanocrystals also permit spectral tunability of their linear and nonlinear optical properties over the entire visible and near-infrared regions. Semiconductor nanocrystals have been demonstrated to exhibit strong saturation of absorption near the excitonic peak associated with the first allowed electronic transition. The nonresonant nonlinear response of nanocrystals is of a similar magnitude as in bulk and in MQW inorganic crystalline semiconductors.

The figures of merit for organic materials in the absorbing region are in general poor. In the transparent region the Kerr and two-photon absorption coefficients of organic materials are of magnitudes comparable to these of inorganic crystalline semiconductors. The sign of the refractive nonlinearity varies across the spectrum depending on the proximity to various absorption resonances.

Although the nonlinear properties of many materials systems have been reported, further characterization is needed to assess the applicability of various nonlinear material systems to optical signal processing. In contrast to previously reported measurements carried out at isolated wavelengths, measurements of the refractive and absorptive nonlinear response over wide spectral ranges, which would permit determination of figures of merit, need to be carried out. In particular, the refractive and absorptive nonlinear response in the most-promising absorption-edge regions of MQW semiconductors and semiconductor nanocrystals should be examined comprehensively and the applicability of these material systems to optical signal processing should be determined.

References

45.1 E. Cotter, J. K. Lucek, D. D. Marcenac: IEEE Commun. Mag. **34**, 90–95 (1997)

45.2 P. P. Mitra, J. B. Stark: Nature **411**, 1027 (2001)

45.3 P. W. Smith: The Bell Syst. Tech. J. **61**, 1975–1983 (1982)

45.4 L. Brzozowski, E. H. Sargent: J. Opt. Soc. Am. B **17**, 1360–1365 (2000)

45.5 L. Brzozowski, E. H. Sargent: IEEE J. Quantum Electron. **36**, 550–555 (2000)

45.6 L. Brzozowski, E. H. Sargent: IEEE J. Quantum Electron. **36**, 1237–1242 (2000)

45.7 P. W. Smith, I. P. Kaminov, P. J. Maloney, L. W. Stulz: Appl. Phys. Lett. **34**, 62–65 (1979)

45.8 P. W. Smith, E. H. Turner: Appl. Phys. Lett. **30**, 280–281 (1977)

45.9 B. E. A. Saleh, M. C. Teich: *Fundamentals of Photonics* (Wiley, New York 1991)

45.10 P. W. E. Smith, L. Qian: IEEE Circuits Dev. Mag. **15**, 28–33 (1999)

45.11 P. W. E. Smith: All-optical devices: materials requirements. In: *Nonlinear Optical Properties of Advanced Materials*, Vol. 1852 (SPIE, Los Angeles, CA 1993) pp. 2–9

45.12 G. I. Stegeman: All-optical devices: materials requirements. In: *Nonlinear Optical Properties of Advanced Materials*, Vol. 1852 (SPIE, Los Angeles, CA 1993) pp. 75–89

45.13 I. C. Khoo, M. Wood, B. D. Guenther: *Nonlinear liquid crystal optical fiber array for all-optical switching/limiting*, In: LEOS 96 9th Annual Meeting, Vol. 2, pp. 211–212, IEEE, (Bellingham, 1996)

45.14 G. L. Wood, W. W. II. I. Clark, M. J. Miller, G. J. Salamo, E. J. Sharp: Evaluation of passive optical limiters and switches. In: *Materials for Optical Switches, Isolators, and Limiters*, Vol. 1105 (SPIE, Orlando, FL 1989) pp. 154–181

45.15 R. Bozio, M. Meneghetti, R. Signorini, M. Maggini, G. Scorrano, M. Prato, G. Brusatin, M. Guglielmi: Optical limiting of fullerene derivatives embedded in sol–gel materials, In: Photoactive Organic Materials. Science and Applications, Proc. NATO Adv.

Res. Workshop, Avignon, France, June 25–30, 1995 (Kluwer, Dordrecht 1996) 159–174
45.16 J. A. Hermann, P. B. Chapple, J. Staromlynska, P. Wilson: Design criteria for optical power limiters. In: *Nonlinear Optical Materials for Switching and Limiting*, Vol. 2229, ed. by M. J. Soileau (SPIE, Orlando, FL 1994) pp. 167–178
45.17 N. G. R. Broderick, D. Taverner, D. J. Richardson: Opt. Express **3**, 447–453 (1998)
45.18 N. D. Sankey, D. F. Prelewitz, T. G. Brown: Appl. Phys. Lett. **60**, 1427–1429 (1992.)
45.19 L. Brzozowski, E. H. Sargent: IEEE J. Lightwave Technol. **19**, 114–119 (2000)
45.20 L. Brzozowski, V. Sukhovatkin, E. H. Sargent, A. SpringThorpe, M. Extavour: IEEE J. Quantum Electron. **39**, 924–930 (2003)
45.21 H. M. Gibbs, S. L. McCall, T. N. C. Venkatesan, A. C. Gossard, A. Passner, W. Wiegmann: Appl. Phys. Lett. **35**, 451–453 (1979)
45.22 H. M. Gibbs, S. S. Tang, J. L. Jewell, D. A. Winberger, K. Tai, A. C. Gossard, S. L. McCall, A. Passner: Appl. Phys. Lett. **41**, 221–222 (1982)
45.23 H. G. Winful, J. H. Marburger, E. Garmire: Appl. Phys. Lett. **35**, 379–381 (1979)
45.24 D. Pelinovsky, L. Brzozowski, E. H. Sargent: Phys. Rev. E **60**, R4536–R4539 (2000)
45.25 D. Pelinovsky, J. Sears, L. Brzozowski, E. H. Sargent: J. Opt. Soc. Am. B **19**, 45–53 (2002)
45.26 C. M. de Sterke, J. E. Sipe: Progress Opt. **33**, 203–260 (1994)
45.27 W. Chen, D. L. Mills: Phys. Rev. Lett. **58**, 160–163 (1987)
45.28 W. N. Ye, L. Brzozowski, E. H. Sargent, D. Pelinovsky: J. Opt. Soc. Am. B **20**, 695–705 (2003)
45.29 R. W. Boyd: *Nonlinear Optics* (Academic, New York 1992)
45.30 M. G. Kuzyk, C. W. Dirk: *Characterization Techniques and Tabulations for Organic Nonlinear Optical Materials* (Dekker, New York, N.Y. 1998)
45.31 D. L. Mills: *Nonlinear Optics: Basic Concepts* (Springer, Berlin, Heidelberg 1998)
45.32 P. Gunter: *Nonlinear Optical Effects and Materials* (Springer, Berlin, Heidelberg 2000)
45.33 P. N. Prasad, D. J. Williams: *Introduction to Nonlinear Optical Effects in Molecules and Polymers* (Wiley, New York 1991)
45.34 R. L. Sutherland: *Handbook of Nonlinear Optics* (Dekker, New York 1996)
45.35 E. Garmire: IEEE J. Selected Topics Quantum Electron. **6**, 1094–1110 (2000)
45.36 E. W. Van Stryland, M. A. Woodall, H. Vanherzeele, M. J. Soileau: Opt. Lett. **10**, 490–492 (1985)
45.37 M. Sheik-Bahae, D. C. Hutchings, D. J. Hagan, E. W. Van Stryland: IEEE J. Quantum Electron. **27**, 1296–1309 (1991)
45.38 S. H. Park, J. F. Morhange, A. D. Jeffery, R. A. Morgan, A. Chevez-Pirson, H. M. Gibbs, S. W. Koch, N. Peyghambarian, M. Derstine, A. C. Gossard, J. H. English, W. Weigmann: Appl. Phys. Lett. **52**, 1201–1203 (1988)
45.39 L. Qian, S. D. Benjamin, P. W. E. Smith, H. Pinkney, B. J. Robinson, D. A. Thompson: Opt. Lett. **22**, 108–110 (1997)
45.40 H. S. Loka, S. D. Benjamin, P. W. E. Smith: IEEE J. Quantum Electron. **34**, 1426–1437 (1998)
45.41 H. Pinkney, D. A. Thompson, B. J. Robinson, L. Qian, S. D. Benjamin, P. W. E. Smith: J. Cryst. Growth **209**, 237–241 (2000)
45.42 S. Gupta, M. Y. Frankel, J. A. Valdmanis, J. F. Whitaker, G. A. Mourou, F. W. Smith, A. R. Calawa: Appl. Phys. Lett. **59**, 3276–3278 (1991)
45.43 E. S. Harmon, M. R. Melloch, J. W. Woodall, D. D. Nolte, N. Olsuka, C. L. Chang: Appl. Phys. Lett. **63**, 2248–2250 (1993)
45.44 S. D. Benjamin, A. Othonos, P. W. E. Smith: Electron. Lett. **30**, 1704–1706 (1994)
45.45 P. W. E. Smith, S. D. Benjamin, H. S. Loka: Appl. Phys. Lett. **71**, 1156–1158 (1997)
45.46 M. Kawase, E. Garmire, H. C. Lee, P. D. Dapkus: IEEE J. Quantum Electron. **30**, 981–988 (1994)
45.47 L. Brzozowski, E. H. Sargent, A. SpringThorpe, M. Extavour: Appl. Phys. Lett. **82**, 4429–4431 (2003)
45.48 D. A. B. Miller, D. S. Chemla, D. J. Eilenbergeer, P. W. Smith, A. C. Gossard, W. T. Tsang: Appl. Phys. Lett. **41**, 679–681 (1982)
45.49 S. Schmitt-Rink, D. S. Chemla, D. A. B. Miller: Phys. Rev. B **32**, 6601–6609 (1985)
45.50 Y. H. Lee, A. Chavez-Pirson, S. W. Koch, H. M. Gibbs, S. H. Park, J. Morchange, A. Jeffery, N. Peyghambrian, J. Banyai, A. C. Gossard, W. Wiegmann: Phys. Rev. Lett. **57**, 2446–2449 (1986)
45.51 F. Stern: Phys. Rev. **133**, A1653–A1664 (1964)
45.52 A. M. Fox, A. C. Maciel, J. F. Ryan, M. D. Scott: Nonlinear excitonic optical absorption in GaInAs/InP quantum wells
45.53 A. M. Fox, A. C. Maciel, M. G. Shorthose, J. F. Ryan, M. D. Scott, J. I. Davies, J. R. Riffat: Nonlinear excitonic optical absorption in GaInAs/InP quantum wells
45.54 L. Brzozowski, E. H. Sargent, A. SpringThorpe, M. Extavour: Appl. Phys. Lett., 4429–4431 (2003)
45.55 L. Brzozowski, E. H. Sargent, A. SpringThorpe, M. Extavour: Virtual J. Ultrafast Sci. **2**(7) (2003)
45.56 P. W. Joudawlkis, D. T. McInturff, S. E. Ralph: Appl. Phys. Lett. **69**, 4062–4064 (1996)
45.57 R. V. Penty, H. K. Tsang, I. H. White, R. S. Grant, W. Sibert, J. E. A. Whiteaway: Electron. Lett. **27**, 1447–1449 (1991)
45.58 I. E. Day, P. A. Snow, R. V. Penty, I. H. White, R. S. Grant, G. T. Kennedy, W. Sibbett, D. A. O. Davies, M. A. Fisher, M. J. Adams: Appl. Phys. Lett. **65**, 2657–2659 (1994)
45.59 M. A. Fisher, H. Wickes, G. T. Kennedy, R. S. Grant, W. Sibbett: Electron. Lett. **29**, 1185–1186 (1993)
45.60 D. A. O. Davies, M. A. Fisher, D. J. Elton, S. D. Perrin, M. J. Adams, G. T. Kennedy, R. S. Grant,

P. D. Roberts, W. Sibbett: Electron. Lett. **29**, 1710–1711 (1993)
45.61 C. Aversa, J. E. Sipe, M. Sheik-Bahae, E. W. V. Stryland: Phys. Rev. B **24**, 18073–18082 (1994)
45.62 M. J. Shaw, M. Jaros: Phys. Rev. B **47**, 1620–1623 (1993)
45.63 K. S. Bindra, A. K. Kar: Appl. Phys. Lett. **79**, 3761–3763 (2001)
45.64 M. Sheik-Bahae, D. J. Hagan, E. W. Van Stryland: Phys. Rev. Lett. **65**, 96–99 (1990)
45.65 N. J. Long: Angew. Chem., Int. Ed. **34**, 21–38 (1995)
45.66 I. Liakatas, C. Cai, M. Bösch, C. B. M. Jäger, P. Günter: Appl. Phys. Lett. **76**, 1368–1370 (2000)
45.67 R. Rangel-Rojo, S. Yamada, H. Matsuda, D. Yankelevicg: Appl. Phys. Lett. **72**, 1021–1023 (1998)
45.68 R. Rangel-Rojo, S. Yamada, H. Matsuda, H. Kasai, H. Nakanishi, A. K. Kar, B. S. Wherrett: J. Opt. Soc. Am. B **203**, 2937–2945 (1998)
45.69 R. Rangel-Rojo, S. Yamada, H. Matsuda, H. Kasai, Y. Komai, S. Okada, H. Oikava, H. Nakanishi: Jap. J. Appl. Phys. **38**, 69–73 (1999)
45.70 R. Rangel-Rojo, H. Matsuda, H. Kasai, H. Nakanishi: J. Opt. Soc. Am. **17**, 1376–1382 (2000)
45.71 E. Van Keuren, T. Wakebe, R. Andreaus, H. Möhwald, W. Schrof, V. Belov, H. Matsuda, R. Rangle-Rojo: J. Opt. Soc. Am. B **203**, 2937–2945 (1998)
45.72 R. Rangel-Rojo, L. Stranges, A. K. Kar, M. A. Mendez-Rojas, W. H. Watson: Opt. Commun. **203**, 385–391 (2002)
45.73 L. Demenicis, A. S. L. Gomes, D. V. Petrov, C. B. de Araújo, C. P. de Molo, C. G. dos Santos, R. Souto-Major: J. Opt. Soc. Am. B **14**, 609–614 (1997)
45.74 C. Sauteret, J. P. Hermann, R. Frey, F. Pradère, J. Ducling, R. H. Baughman, R. R. Chance: Phys. Rev. Lett. **36**, 956–959 (1976)
45.75 G. P. Agrawal, C. Cojan, C. Flytzanis: Phys. Rev. B **17**, 776–789 (1978)
45.76 S. R. Marder, B. Kippelen, A. Y. Jan, N. Peyghambarian: Nature **388**, 845–951 (1997)
45.77 B. L. Lawrence, M. Cha, J. U. Kang, W. Torruellas, G. Stegeman, G. Baker, J. Meth, S. Etemad: Electron. Lett. **30**, 447–448 (1994)
45.78 B. L. Lawrence, W. Torruellas, M. C. G. Stegeman, J. Meth, S. Etemad, G. Baker: Electron. Lett. **30**, 447–448 (1994)
45.79 F. Yoshino, S. Polyakov, L. Friedrich, M. Liu, H. Shim, G. I. Stegeman: J. Nonlinear Opt. Phys. Mater. **9**, 95–104 (2000)
45.80 F. Yoshino, S. Polyakov, M. Liu, G. Stegeman: Phys. Rev. Lett. **91**, 063901–1–063901–4 (2003)
45.81 S. Wang, W. Huang, R. Liang, Q. Gong, H. Li, H. Chen, D. Qiang: Phys. Rev. B **63**, 153408(1–4) (2001)
45.82 B. L. Yu, H. P. Xia, C. S. Zhu, F. X. Gan: Appl. Phys. Lett. **81**, 2701–2703 (2002)
45.83 Q. Chen, L. Kuang, E. H. Sargent, Z. Y. Wang: Appl. Phys. Lett. **83**, 2115–2117 (2003)
45.84 F. W. Wise: Accounts Chem. Res. **33**, 773–780 (2000)
45.85 L. Banyai, S. W. Koch: Phys. Rev. Lett. **57**, 2722–2724 (1986)
45.86 S. Schmitt-Rink, D. A. B. Miller, D. S. Chemla: Phys. Rev. B **35**, 8113–8125 (1987)
45.87 M. A. Hines, G. D. Scholes: Synthesis of colloidal PbS nanocrystals with size-tunable NIR emissions, submitted
45.88 G. Wang, K. Guo: Physica B **315**, 234–239 (2001)
45.89 P. T. Guerreiro, S. Ten, N. F. Borrelli, J. Butty, G. E. Jabbour, N. Peyghambarian: Appl. Phys. Lett. **71**, 1595–1597 (1997)
45.90 K. Wundke, S. Pötting, J. Auxier, A. Schülzgen, N. Pegyghambarian, N. F. Borrelli: Appl. Phys. Lett. **76**, 10–12 (2000)
45.91 A. M. Malyarevich, V. G. Savitski, P. V. Prokoshin, N. N. Posonov, K. V. Yumashev, E. Raaben, A. A. Zhilin: J. Chem. Phys. **78**, 1543–1551 (1983)
45.92 D. Cotter, M. C. Burt, R. J. Manning: Phys. Rev. Lett. **68**, 1200–1203 (1992)
45.93 H. P. Li, B. Liu, C. H. Kam, Y. L. Lam, W. X. Que, L. M. Gan, C. H. Chew, G. Q. Xu: Opt. Mater. **14**, 321–327 (2000)
45.94 B. Liu, H. Li, C. H. Chew, W. Que, Y. L. Lam, C. H. Kam, L. M. Gan, G. Q. Xu: Mater. Lett. **51**, 461–469 (2001)
45.95 B. Liu, C. H. Chew, L. M. Gan, G. Q. Xu, H. Li, Y. L. Lam, C. H. Kam, W. X. Que: Mater. Lett. **51**, 461–469 (2001)
45.96 L. Yang, K. Becker, F. M. Smith, R. H. Magruder III, R. F. Haglund Jr., L. Yang, R. Dorsinville, R. R. Alfano, R. A. Zuhr: Size dependence of the third-order susceptibility of copper nanocrystals investigated by four-wave mixing
45.97 K. Uchida, S. Kaneko, S. Omi, C. Hata, H. Tanji, Y. Asahara, A. J. Ikushima, T. Tokizaki, A. Nakamura: J. Opt. Soc. Am. **11**, 1236–1243 (1994)
45.98 H. Inouye, K. Tanaka, I. Tanahashi, T. Hattori, H. Nakatsuka: Jap. J. Appl. Phys. **39**, 5132–5133 (2000)
45.99 D. Ricard, P. Roussignol, C. Flytanis: Opt. Lett. **10**, 511–513 (1985)
45.100 D. V. Petrov: Opt. Commun. **13**, 102–106 (1996)
45.101 C. Bosshard: Adv. Mater. **5**, 385–397 (1996)
45.102 G. I. Stegeman, D. J. Hagan, L. Torner: Opt. Quantum Electron. **28**, 1691–1740 (1996)